J Arid Land (2024) 16(10): 1303–1326
doi: 10.1007/s40333-024-0086-z; CSTR: 32276.14.JAL.0240086z

Science Press Springer-Verlag

# Spatiotemporal evolution and future simulation of land use/land cover in the Turpan-Hami Basin, China

CHEN Yiyang[1,2,3], ZHANG Li[1,2*], YAN Min[1,2], WU Yin[4], DONG Yuqi[1,2,3], SHAO Wei[1,5], ZHANG Qinglan[1,6]

[1] Key Laboratory of Digital Earth Science, Aerospace Information Research Institute, Chinese Academy of Sciences, Beijing 100094, China;
[2] International Research Center of Big Data for Sustainable Development Goals, Beijing 100094, China;
[3] University of Chinese Academy of Sciences, Beijing 100094, China;
[4] Xinjiang Uygur Autonomous Region Natural Resources Planning and Research Institute, Urumqi 830011, China;
[5] School of Geomatics and Marine Information, Jiangsu Ocean University, Lianyungang 222001, China;
[6] College of Geomatics and Geoinformation, Guilin University of Technology, Guilin 541004, China

**Abstract:** The Turpan-Hami (Tuha) Basin in Xinjiang Uygur Autonomous Region of China, holds significant strategic importance as a key economic artery of the ancient Silk Road and the Belt and Road Initiative, necessitating a holistic understanding of the spatiotemporal evolution of land use/land cover (LULC) to foster sustainable planning that is tailored to the region's unique resource endowments. However, existing LULC classification methods demonstrate inadequate accuracy, hindering effective regional planning. In this study, we established a two-level LULC classification system (8 primary types and 22 secondary types) for the Tuha Basin. By employing Landsat 5/7/8 imagery at 5-a intervals, we developed the LULC dataset of the Tuha Basin from 1990 to 2020, conducted the accuracy assessment and spatiotemporal evolution analysis, and simulated the future LULC under various scenarios via the Markov-Future Land Use Simulation (Markov-FLUS) model. The results revealed that the average overall accuracy values of our LULC dataset were 0.917 and 0.864 for the primary types and secondary types, respectively. Compared with the seven mainstream LULC products (GlobeLand30, Global 30-meter Land Cover with Fine Classification System (GLC_FCS30), Finer Resolution Observation and Monitoring of Global Land Cover PLUS (FROM_GLC PLUS), ESA Global Land Cover (ESA_LC), Esri Land Cover (ESRI_LC), China Multi-Period Land Use Land Cover Change Remote Sensing Monitoring Dataset (CNLUCC), and China Annual Land Cover Dataset (CLCD)) in 2020, our LULC data exhibited dramatically elevated overall accuracy and provided more precise delineations for land features, thereby yielding high-quality data backups for land resource analyses within the basin. In 2020, unused land (78.0% of the study area) and grassland (18.6%) were the dominant LULC types of the basin; although cropland and construction land constituted less than 1.0% of the total area, they played a vital role in arid land development and primarily situated within oases that form the urban cores of the cities of Turpan and Hami. Between 1990 and 2020, cropland and construction land exhibited a rapid expansion, and the total area of water body decreased yet resurging after 2015 due to an increase in areas of reservoir and pond. In future scenario simulations, significant increases in areas of construction land and cropland are anticipated under the business-as-usual scenario, whereas the wetland area will decrease, suggesting the need for ecological attention under this development pathway. In contrast, the economic development scenario underscores the fast-paced expansion of construction land, primarily from the conversion of unused land, highlighting the significant developmental potential of unused land with a slowing increase in cropland. Special attention should thus be directed toward ecological and cropland protection during development. This study provides data supports and policy recommendations for the sustainable development goals of Tuha Basin and other similar arid areas.

*Corresponding author: ZHANG Li (E-mail: zhangli@aircas.ac.cn)
Received 2024-05-31; revised 2024-09-03; accepted 2024-09-06

**Keywords:** land use/land cover (LULC); future simulation; manual interpretation; Markov-Future Land Use Simulation (Markov-FLUS) model; Turpan-Hami (Tuha) Basin; Xinjiang

**Citation:** CHEN Yiyang, ZHANG Li, YAN Min, WU Yin, DONG Yuqi, SHAO Wei, ZHANG Qinglan. 2024. Spatiotemporal evolution and future simulation of land use/land cover in the Turpan-Hami Basin, China. Journal of Arid Land, 16(10): 1303–1326. https://doi.org/10.1007/s40333-024-0086-z; https://cstr.cn/32276.14.JAL.0240086z

## 1 Introduction

As a unique geographical and climatic landscape, arid areas cover more than 40.0% of the global land surface. Owing to the fragile ecological environment and limited resource-carrying capacity, especially the scarcity of water resources, the contradiction between development and protection is particularly prominent in arid areas (Wang et al., 2023). The land use/land cover (LULC) of arid areas is influenced by various factors, including climate fluctuations, hydrological changes, and the human utilization of natural resources. These factors contribute to the complexity and diversity of LULC, as well as its sensitivity in response to environmental variations. Therefore, understanding the changes in LULC, further analyzing their impacts on ecosystems, and exploring effective pathways to mitigate adverse effects are crucial for promoting the harmonisation of the natural environment and socio-economic development (Schirpke et al., 2020).

Currently, China's arid areas face significant challenges related to land degradation. While large-scale vegetation restoration programs implemented since 1978 have significantly improved or greened 45.8% of the drylands in China, these initiatives also exert substantial water pressure. Therefore, China's arid areas continue to experience land degradation and intensified aridity (Li et al., 2021). Xinjiang Uygur Autonomous Region (hereinafter referred to as Xinjiang), located in the core of the global arid areas, is an ideal place for studying these phenomena. Xinjiang is renowned not only for its vast land and diverse natural landscapes but also for its diverse ecosystems and human lifestyles, and thus has resulted in a rich array of LULC types (Xu et al., 2019). In recent years, scholars have delved into pertinent investigations concerning the LULC in this region (Chen et al., 2020a; Yimuranjiang et al., 2021). Among the many unique regions in Xinjiang, Turpan-Hami (Tuha) Basin stands out for its distinctive desert features. The Tuha Basin has unique geographical and climatic conditions, with more than 70.0% of its land classified as unused land and less than 10.0% designated for agriculture, orchards, forests, and urban areas. Although oases cover only 8.0% of the basin, they are the primary drivers of local economy, with over 95.0% of population and agricultural gross domestic product (GDP). This LULC pattern indicates significant potential for future development but also presents severe challenges, such as water scarcity and high desertification levels. Water scarcity is a critical limiting factor for LULC changes in this region, and special land uses such as mining areas and photovoltaic sites exacerbate this issue. Furthermore, urban expansion has led to a decline in dryland habitat quality, highlighting the critical importance of strategic management in mitigating the significant impact of urbanization on biodiversity (Ren et al., 2022). Therefore, it is crucial to study the LULC changes in the Tuha Basin for formulating effective development plans.

Research on LULC has its roots in conventional surveys and cartography. In the 1990s, the establishment of the International Geosphere and Biosphere Program and the Global Change and Human Dimensions Program marked pivotal moments. Presently, integrated LULC surveys have gained increasing importance in both regional and global sustainable development contexts. Crucially, various pressing global challenges linked to LULC changes, such as climate change, biodiversity loss, and the exacerbation of desertification, underscore the pivotal role of these surveys (Kuang et al., 2022; Luo and Zhang, 2022). Currently, commonly used global LULC products include the GlobeLand30 from the National Geomatics Center of China (Chen et al., 2015b), Global 30-meter Land Cover with Fine Classification System (GLC_FCS30) produced by the Aerospace Information Innovation Research Institute of the Chinese Academy of Sciences (Zhang et al., 2021), Finer Resolution Observation and Monitoring of Global Land Cover PLUS (FROM_GLC PLUS) (Yu et al., 2022), ESA global land cover (ESA_LC) (Zanaga et al., 2021),

and Esri Land Cover (ESRI_LC) (Karra et al., 2021). The LULC products in China include the China Multi-Period Land Use Land Cover Change Remote Sensing Monitoring Dataset (CNLUCC) led by the Institute of Geographic Sciences and Natural Resources Research of the Chinese Academy of Sciences (Xu et al., 2018) and China Annual Land Cover Dataset (CLCD) from Wuhan University (Yang and Huang, 2021). These LULC products have been widely applied in fields such as land management, urban expansion, and ecological environment monitoring. However, these products are primarily designed for global and national scales and may not fully suit the classification system in the Tuha Basin. Additionally, these methods lack secondary class refinements tailored to differences in natural attributes, coverage characteristics, and land use, and suffer from issues such as insufficient training samples and low classification accuracy in the Tuha Basin. To address this requirement, this study developed a comprehensive and detailed two-level LULC classification system. This system not only effectively categorized construction land, considering special land uses such as mining areas and photovoltaic sites to meet regional management needs, but also delineated grassland, unused land, and water body. The LULC maps were meticulously developed through manual interpretation of satellite imagery, which is crucial for accurately capturing the unique characteristics of the region and ensuring the precision needed for effective classification. Consequently, the classification results support biodiversity conservation and efforts to combat desertification.

Changes in LULC are complex and dynamic, and studies related to it requires delineation of the historical evolution and its natural and anthropogenic-driven characteristics as well as looking to the future (He et al., 2022). With respect to the historical evolution, scholars have focused on the impacts of LULC changes on climate, soil, water quality, and ecosystem services (Chen et al., 2015a; Bi et al., 2018; Özşahin and Eroğlu, 2019; Dong and Liu, 2022), and have applied spatiotemporal evolution analysis to LULC change patterns (Alijani et al., 2020). Through the combination of these multidisciplinary approaches, research continues to unravel the complex interplay between humans and their environment, offering strategic insights for sustainable land management and policy development. In recent years, future simulation of LULC and the anticipation of variations in the number of LULC types have emerged as captivating areas of concentration in LULC research. Future simulation of LULC plays a crucial role in analyzing the causes and consequences of future landscape dynamics concerning socio-economic and environmental drivers. Cellular automata (CA) model is extensively employed for LULC simulations and has been widely utilized in the spatial optimization of land resources and the determination of urban growth boundaries (Chen et al., 2016; Gharbia et al., 2016). However, there has been a drive to close the disparity between macrolevel demand forecasting and local-scale allocation. Additionally, the LULC simulation characteristics in arid areas present unique challenges and opportunities. The Future Land Use simulations (FLUS) model has emerged as a promising solution, which integrates top-down system dynamics with bottom-up CA models through an interactive coupling mechanism. This integration facilitates the synergistic evolution of both sub-models and has been used in extensive applications in LULC simulation and related fields (Hu et al., 2020; Du et al., 2021; Shan et al., 2022). Therefore, this study combined the strengths of the FLUS model and Markov model. The Markov model excels in capturing the transition probabilities of LULC changes over time, providing a solid foundation for forecasting, whereas the FLUS model integrates spatial simulation to account for the spatial distribution and impact of driving factors such as socio-economic development and policy changes. By employing the two models together, we can more accurately forecast future LULC patterns in the Tuha Basin under various scenarios, supporting sustainable development initiatives.

In this study, we developed the LULC dataset in the Tuha Basin at 5-a intervals spanning from 1990 to 2020. The LULC data of this study in 2020 were compared with seven commonly used LULC products (GlobeLand30, GLC_FCS30, FROM_GLC PLUS, ESA_LC, ESRI_LC, CNLUCC, and CLCD) to evaluate the accuracy. Concurrently, a spatiotemporal evolution analysis of LULC was conducted through the examination of land transfer matrices and dynamic

degrees. Additionally, future simulation of LULC was generated to assess the potential impacts of different development scenarios. The LULC dataset serves as a robust foundation for research into the ecologically, environmentally, and socially sustainable development of the Tuha Basin. It is poised to enhance the execution of crucial initiatives pertaining to ecological, agricultural, cultural, and economic advancement within the region.

## 2 Materials

### 2.1 Study area

The Tuha Basin is an important geographic area and economic and cultural center located in the eastern part of Xinjiang, China, with a total area of approximately $2.2\times10^5$ km$^2$. It encompasses Turpan City and Hami City, with Turpan City comprising Gaochang District, Toksun County, and Shanshan County and Hami City including Yizhou District, Barkol Kazakh Autonomous County, and Yiwu County (Fig. 1). The topography of the Tuha Basin is notable for its encirclement by high mountains, with prominent ranges, including Huoyan Mountain, Bogda Mountains, and Moqinwula Mountains. The Tuha Basin features a significant elevation difference of more than 5600.00 m, shaping its characteristic mountain-basin structure. This mountain-basin structure creates special climatic conditions in the basin, with cold and dry winters, hot summers, and relatively low annual precipitation. Aidingkol Lake, which is the lowest point on land in China, lies at the lowest point of the basin, with its surface being 154.31 m below sea level (Wang and Wu, 2003). The Tuha Basin boasts abundant natural resources, albeit with diverse land resource types and high per capita land ownership. However, extensive desertification and large unused land areas contribute to a generally low utilization rate of land resources, indicating significant development potential. Moreover, due to geographical constraints, agricultural cultivation is largely confined to areas around river irrigation areas, which significantly limits the potential for growing staple and cash crops. Economically, the Tuha Basin, as one of the major oil and gas regions in Xinjiang, serves as a significant area for the extraction of energy resources, playing a strategic role in national energy security and regional industrial development. The basin is also known for its agricultural productivity and tourism potential, which contribute to its unique economic profile. Despite notable achievements in economic development, the Tuha Basin faces severe ecological fragility, characterized by extensive land degradation and sparse vegetation. As an essential ecological restoration area in Xinjiang, the quality of its ecological security barrier is crucial for national energy security and the preservation of biodiversity in extremely arid areas (Li et al., 2024). Generally speaking, LULC in the Tuha Basin is undergoing rapid and complex changes, necessitating a comprehensive consideration of the balance between socio-economic development and ecological environment.

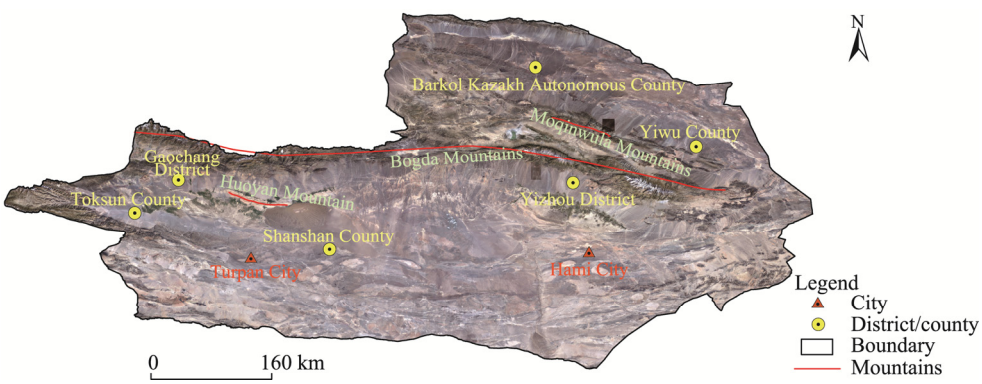


**Fig. 1** Overview of the Turpan-Hami (Tuha) Basin based on the remote sensing images in 2020. The images are sourced from Google Earth (https://www.google.com/). The boundary is based on the standard map (GS (2020)4619) of the Map Service System (https://bzdt.ch.mnr.gov.cn/), and the boundary has not been modified.

### 2.2 Data sources

The image data for LULC classification were the Landsat series T1_SR surface reflectance dataset, which is based on time series analysis of the Google Earth Engine (GEE) platform (https://earthengine.google.com/). Specifically, Landsat TM data were selected for 1990 and 1995, Landsat ETM+ data were used for 2000, 2005 and 2010, and Landsat OLI data were used for 2015 and 2020. All the above data were utilized on the GEE platform after time-phase selection, cloud processing, band synthesis, and cropping, and vegetation growing season images were obtained from March to October.

The LULC product datasets of GLC_FCS30, Globelland30, CLCD, and CNLUCC were obtained from authoritative sources, namely, the CASEarth Thematic Data System (https://data.casearth.cn/thematic/), National Platform for Common Geospatial Information Service (https://data.casearth.cn/), National Cryosphere Desert Data Center (http://www.ncdc.ac.cn/), and Resource and Environment Data Cloud Platform of the Chinese Academy of Sciences (http://www.resdc.cn), respectively. The LULC product datasets of FROM_GLC PLUS, ESA_LC, and ESRI_LC were downloaded from the GEE platform. These seven datasets were utilized for the comparative analysis of LULC data for the year 2020.

The driving factors for the LULC simulation model consisted primarily of Shuttle Radar Terrain Mission digital elevation model (SRTM DEM; m) data with a 30-m resolution, which were obtained from the Earth Explorer (https://earthexplorer.usgs.gov/). Subsequently, aspect (°) and slope (°) calculations were executed via the GEE. The monthly precipitation (mm) and temperature (°C) data with a 1-km resolution were downloaded from the National Earth System Science Data Center (http://www.geodata.cn/). The socio-economic data, including GDP ($\times 10^6$ CNY) and 1 km gridded human population distribution (HPD; pcs) in 2020, were obtained from the National Earth System Science Data Center and the WorldPOP (https://hub.worldpop.org/), respectively. The road network data were sourced from the 1:1,000,000 public version of the National Catalogue Service for Geographic Information (https://www.webmap.cn/). The above datasets were processed into 1 km data.

## 3 Methods

This study established a comprehensive LULC classification system for the Tuha Basin, utilizing remote sensing interpretation with a 30-m resolution. The derived LULC dataset covered years of 1990, 1995, 2000, 2005, 2010, 2015, and 2020. The overall accuracy and kappa coefficient was employed for accuracy assessment of the LULC dataset, whereas the user accuracy and producer accuracy metrics were used to evaluate the classification quality of each LULC types. The derived LULC data in 2020 were then compared against the seven mainstream product datasets. Furthermore, we conducted the spatiotemporal evolution analysis by employing land transition matrices and dynamic degrees and future LULC simulations for different scenarios on the basis of the Markov-Future Land Use Simulation (Markov-FLUS) model. Figure 2 gives the flow diagram of the study.

### 3.1 LULC classification

#### 3.1.1 Classification system and method

To establish a robust LULC classification system, we referred to the CNLUCC, Technical Regulations for the Third National Land Survey, and national standard GB/T 21010-2017 (https://std.samr.gov.cn/). A two-level LULC classification system was then developed considering LULC characteristics, onsite inspections, and the feasibility of remote sensing image interpretation in the Tuha Basin (Table 1). At the first level, the system comprised eight primary LULC types based on the LULC characteristics and dominant functions, including cropland, orchard, woodland, grassland, wetland, water body, construction land, and unused land. The second level further refined the primary LULC types into 22 secondary LULC types, considering natural attributes, coverage characteristics, and land use differences.

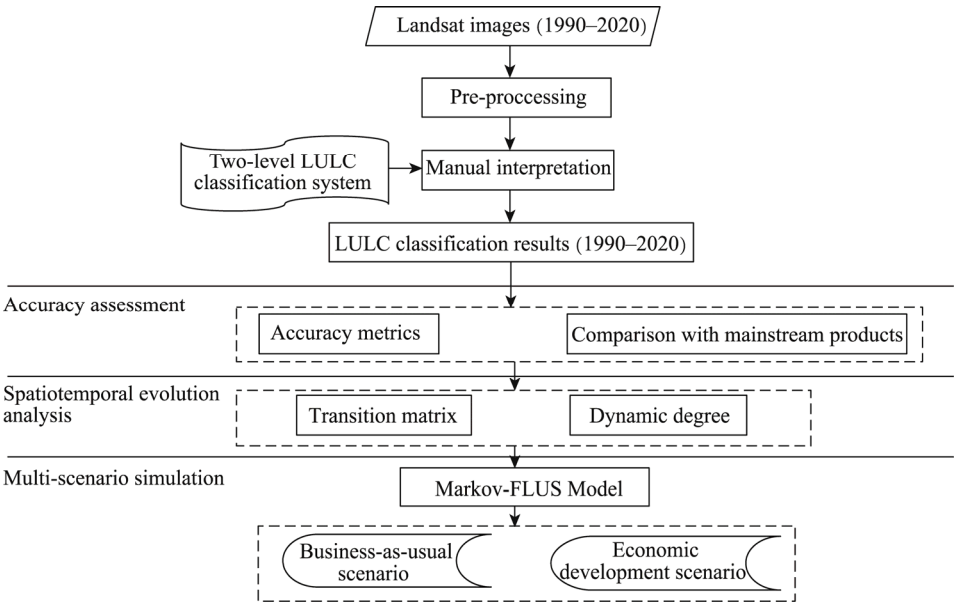


**Fig. 2** Flow diagram of the study. LULC, land use/land cover; Markov-FLUS, Markov-Future Land Use Simulation.

**Table 1** Classification system of land use/land cover (LULC) in the study

| ID | Primary LULC type | ID | Secondary LULC type | ID | Primary LULC type | ID | Secondary LULC type |
|---|---|---|---|---|---|---|---|
| 1 | Cropland | - | - | 7 | Construction land | 71 | Urban residential area |
| 2 | Orchard | - | - | | | 72 | Rural residential area |
| 3 | Woodland | 31 | Forestland | | | 73 | Mining land |
| | | 32 | Shrub land | | | 74 | Wind power and photovoltaic land |
| | | 33 | Sparse woodland | | | 75 | Other construction land |
| | | 34 | Other woodland | 8 | Unused land | 81 | Sandy land |
| 4 | Grassland | 41 | High-coverage grassland | | | 82 | Gobi |
| | | 42 | Mid-coverage grassland | | | 83 | Saline–alkali land |
| | | 43 | Low coverage grassland | | | 84 | Bare land |
| 5 | Wetland | - | - | | | 85 | Bare rocky land |
| 6 | Water body | 61 | River | | | 86 | Other unused land |
| | | 62 | Lake | | | | |
| | | 63 | Reservoir and pond | | | | |
| | | 64 | Permanent glacier | | | | |

Note: "-" indicates no corresponding ID or secondary LULC type.

In this study, a manual interpretation method was used for LULC classification based on time series Landsat data. To ensure the accuracy of the results, high-resolution imagery from Google Earth was used to clarify ambiguous areas in the Landsat images. Additionally, topological checks were performed to fill in missing positions and adjust overlapping polygons, ensuring the overall reasonableness and reliability of the data.

### 3.1.2 Accuracy assessment

In this study, the sample point distribution was determined on the basis of the verification data in 2020, with a total of 1800 sample points stratified randomly selected for accuracy assessment. This distribution included 1000 sample points for unused land, 200 sample points for grassland,

and 100 sample points for each of the other LULC types. After establishing this distribution with the verification data in 2020, the attributes of the sample points for other years were determined on the basis of their respective verification data. Specifically, the verification for 2010, 2015, and 2020 relied primarily on Nationwide Land and Resources Survey result data, whereas for other years, if significant differences were observed in the images, sample attributes were adjusted on the basis of the Xinjiang LULC product data provided by the National Cryosphere Desert Data Center (http://www.ncdc.ac.cn/). However, owing to differences in classification systems, the samples were adjusted to align with the classification system used in this study, and incorrect sample attributes were corrected via high-resolution imagery from Google Earth. Evaluating the accuracy of land cover products is necessary before further analysis can be performed (Olofsson et al., 2013). Previous research has indicated that confusion matrices are commonly regarded as the optimal method for accuracy assessment (Gómez et al., 2016). Through confusion matrices, quantitative metrics such as user accuracy, producer accuracy, overall accuracy, and kappa coefficient can be calculated to measure the overall performance of LULC dataset. The calculation formulas are as follows:

$$\mathrm{UA} = \frac{\mathrm{TP}}{\mathrm{TP} + \mathrm{FP}}, \tag{1}$$

$$\mathrm{PA} = \frac{\mathrm{TP}}{\mathrm{TP} + \mathrm{FN}}, \tag{2}$$

$$\mathrm{OA} = \frac{\mathrm{TP} + \mathrm{TN}}{\mathrm{TP} + \mathrm{TN} + \mathrm{FP} + \mathrm{FN}}, \tag{3}$$

$$\mathrm{Kappa} = \frac{\mathrm{OA} - \mathrm{Pe}}{1 - \mathrm{Pe}}, \tag{4}$$

$$\mathrm{Pe} = \frac{(\mathrm{TP} + \mathrm{FN}) \times (\mathrm{TP} + \mathrm{FP}) + (\mathrm{FP} + \mathrm{TN}) \times (\mathrm{FN} + \mathrm{TN})}{(\mathrm{TP} + \mathrm{TN} + \mathrm{FP} + \mathrm{FN})^2}, \tag{5}$$

where UA is the user accuracy, which refers to the proportion of correctly classified samples to the total number of samples; TP represents the true positives (samples correctly classified as positive); FP represents the false-positives (samples incorrectly classified as positive); PA is the producer accuracy, which represents the proportion of samples correctly classified within the true class; FN represents the false-negatives (samples incorrectly classified as negative); OA is the overall accuracy, which is the proportion of correctly classified samples to the total number of samples; TN represents the true negatives (samples correctly classified as negative); Kappa represents the kappa coefficient, which is a ratio representing the proportion of error reduction in classification compared with completely random classification; and Pe is the expected agreement, calculated as the sum of the products of the actual and predicted counts for each class, divided by the square of the total number of samples.

In the accuracy assessment part of this study, a comparison was also made between the LULC data produced by this study in 2020 and the seven mainstream LULC products.

### 3.2 Spatiotemporal evolution analysis of LULC based on land transition matrix and dynamic degree index

This study involves a statistical analysis of LULC dynamics from 1990–2020 via land transition matrix and dynamic degree index. The transition matrix was structured to illustrate the transitions occurring between distinct LULC types during the specified time period, presenting a systematic representation of the LULC dynamics. All area calculations were based on the WGS 1984 UTM Zone 43N projected coordinate system. The formula for the transition matrix is as follows:

$$A=\begin{bmatrix} A_{11} & A_{12} & \cdots & A_{1j} \\ A_{21} & A_{22} & \cdots & A_{2j} \\ \vdots & \cdots & \ddots & \vdots \\ A_{i1} & A_{i1} & \cdots & A_{ij} \end{bmatrix}, \tag{6}$$

where $A$ is the transition matrix; and $A_{ij}$ is the land area of transition from LULC type $i$ to $j$ (km$^2$).

The regional disparities in the rates of LULC change can be reflected by dynamic degree. This study utilized the dynamic degree index proposed by Liu et al. (2010). The single dynamic degree and the comprehensive dynamic degree were separately computed for each LULC type to depict the individual characteristics of LULC dynamics for each LULC type and the overall comprehensive features of LULC transformation in the Tuha Basin from 1990 to 2020. The formula for a single dynamic degree is as follows:

$$\mathrm{SD}=\frac{U_b-U_a}{U_a}\times\frac{1}{T}\times 100\%, \tag{7}$$

where SD represents the single dynamic degree (%); $U_a$ represents the land area in the initial year $a$ (km$^2$); $U_b$ denotes the land area in the current year $b$ (km$^2$); and $T$ represents the time interval from $a$ to $b$.

The formula for the comprehensive dynamic degree is as follows:

$$\mathrm{CD}=\frac{\sum_{i=1}^{n}\left|U_{ib}-U_{ia}\right|}{A}\times\frac{1}{T}\times 100\%, \tag{8}$$

where CD represents the comprehensive dynamic degree (%); $n$ represents the number of LULC types; $U_{ia}$ represents the area of LULC type $i$ in the initial year $a$ (km$^2$); $U_{ib}$ represents the area of land use type $i$ in the current year $b$ (km$^2$); $A$ represents the total area of the study area (km$^2$); and $T$ represents the time period in years.

### 3.3 Scenario simulation analysis based on the Markov-FLUS model

This study employed the Markov-FLUS model to simulate the LULC in the Tuha Basin for the years 2030, 2040, and 2050 under business-as-usual and economic development scenarios. Initially, land expansion patterns were determined via the Markov model. The FLUS model was subsequently utilized to simulate these expansion patterns spatially. When the FLUS model was used, the process was initiated by assessing the weight of neighborhood influence to determine the capability for land expansion based on existing LULC patterns. Then, the land suitability probability was evaluated through an artificial neural network (ANN) model. Finally, the development models were configured in alignment with varying scenarios to facilitate forecasting via the model. In our study, we employed the root mean square error (RMSE) to assess the adequacy of fit for the ANN model in simulating land suitability probabilities. Additionally, the kappa coefficient was used to validate the overall simulation accuracy of the model when it forecasted the LULC data in 2020 on the basis of the LULC data in 2010.

#### 3.3.1 Scenario settings

The business-as-usual scenario represents a baseline where existing trends and practices continue without significant policy or management interventions. On the basis of the LULC change patterns from 2010 to 2020, the Markov model was used to simulate the future scale of each LULC type. These simulations served as scale demand parameters for the FLUS model, allowing for mutual transitions of LULC types. This scenario is essential for understanding natural LULC changes under current conditions and serves as a reference for the rapid economic development scenario.

Rapid economic development is an inevitable trend in the Tuha Basin. The economic development scenario simulates future LULC changes on the basis of anticipated economic activities and growth patterns. To support industrial, commercial, and infrastructure development, the cost matrix was set to prevent the conversion of construction land into other types. Under this scenario, the conversion of construction land accelerated the transitions of other types by 40.0%.

This can ensure the stability and sustainability of construction land, providing a practical framework for stakeholders and policy-makers (Chen et al., 2022b).

**3.3.2** Simulation process

The FLUS model uses a combination of top-down system dynamics and bottom-up CA to significantly enhance its ability to simulate future LULC patterns accurately (Liu et al., 2017). Moreover, the FLUS model employs the ANN algorithms to derive suitability probabilities for various LULC types on the basis of initial LULC data and multiple driving factors, including human activities and natural factors. The model effectively handles the uncertainty and complexity associated with the mutual transitions of LULC types under the combined influence of natural factors and human activities via an adaptive inertia competition mechanism based on roulette wheel selection.

(1) Simulating land expansion patterns via the Markov model. The Markov model simulates future LULC changes on the basis of the transition probability matrix between previous LULC states. This paper simulated the areas of different LULC types at 10-a intervals, and the simulated data served as parameters for the LULC area the FLUS model and were used to calculate neighborhood expansion parameters. To accommodate various scenarios, adjustments were made accordingly. In the business-as-usual scenario, the Markov matrix remained unadjusted. Under the economic development scenario, the conversion of construction land will accelerate the transitions of other types by 40.0%. The specific formula is as follows:

$$S_{(t+1)} = P_{(t-1)t} S_t , \tag{9}$$

where $S_{(t+1)}$ represents the state of LULC at time $t$+1; $P_{(t-1)t}$ represents the transition probability matrix of LULC types from time $t$–1 to $t$; and $S_t$ represents the initial state of LULC at time $t$.

(2) Weights of the neighborhood parameter for setting land expansion capability. The weights of the neighborhood parameter are used to establish the neighborhood factor for different LULC types, with values ranging from 0 to 1. A value closer to 1 indicates a stronger expansion capability for that LULC type. In this study, the Markov-based calculation of land expansion patterns was used to determine the expansion area ratio of each LULC type relative to the total land expansion, thus determining the neighborhood weights for each LULC type.

(3) Calculation of the suitability probability via the ANN model. The suitability probability requires determining the occurrence probability of each LULC type at each pixel within the study area on the basis of LULC data and different driving factors. This is achieved by integrating and computing with the ANN model. LULC changes are the result of the combined actions and driving forces of internal and external factors, such as socio-economic factors, physical and chemical conditions of different LULC types, and natural conditions (Yang et al., 2011). In this study, topographical factors, natural factors, and socio-economic factors served as driving forces. Specifically, topographical factors included DEM, aspect, and slope, whereas natural factors included temperature and precipitation. Socio-economic factors included the GDP, HPD, and distance to main roads.

(4) Generation of cost matrices for different scenarios. The cost matrix indicates whether LULC types can be converted between each other, where 0 represents no conversion and 1 represents that the conversion is possible. In the business-as-usual scenario, mutual transitions of various LULC types were assumed on the basis of past trends without policy restrictions. In the economic development scenario, construction land stability is ensured by preventing its conversion to other types, supporting rapid economic development.

# 4 Results

## 4.1 Evaluation of our LULC dataset in the Tuha Basin

**4.1.1** Accuracy assessment

Table 2 gives the accuracy assessment results for primary and secondary LULC types of our

LULC dataset from 1990 to 2020. In general, the LULC data for each year demonstrated consistent and generally high levels of overall accuracy in both the primary and secondary types. The average overall accuracy of primary LULC types was 0.917, achieving a peak value of 0.946 in 2020. The average kappa coefficient was greater than 0.850 and reached the highest value of 0.918 in 2020, indicating robust performance in classifying the primary LULC types. The overall accuracy of secondary LULC types showed an average value of 0.864, ranging from 0.848 to 0.894. These results underscored the reliability and stability of the LULC classifications over the examined period.

Furthermore, an assessment was conducted on the user accuracy and producer accuracy of different LULC types (Table S1). From the perspective of producer accuracy, unused land, water body, and wetland had relatively high accuracy, followed by orchard and grassland, whereas construction land, cropland, and woodland had relatively lower accuracy. These results suggested that, owing to the utilization of manual interpretation methods, high accuracy can be achieved for unused land, water body and wetland, which possess notably distinct image texture features. Furthermore, we also observed that even though construction land possesses complex texture features, its accuracy following the manual interpretation remained lower. This could be because construction land often contains some smaller buildings, which, although they occupy a small area on the image, can significantly impact the interpretability accuracy. The accuracy of cropland increased significantly after 2010, which can be attributed primarily to the incorporation of the Third National Land Survey data during the interpretation process. The accuracies for other specific LULC types experienced slight fluctuations across different years; however, the overall inter-annual differences in accuracy were not substantial.

**Table 2** Overall accuracy and kappa coefficients for the primary and secondary types of our LULC dataset

| Year | Primary LULC type | | Secondary LULC type | |
|---|---|---|---|---|
| | Overall accuracy | Kappa coefficient | Overall accuracy | Kappa coefficient |
| 1990 | 0.915 | 0.845 | 0.870 | 0.835 |
| 1995 | 0.906 | 0.828 | 0.858 | 0.819 |
| 2000 | 0.911 | 0.839 | 0.862 | 0.825 |
| 2005 | 0.907 | 0.833 | 0.863 | 0.827 |
| 2010 | 0.916 | 0.860 | 0.854 | 0.822 |
| 2015 | 0.919 | 0.871 | 0.848 | 0.817 |
| 2020 | 0.946 | 0.918 | 0.894 | 0.875 |
| Average | 0.917 | 0.856 | 0.864 | 0.831 |

#### 4.1.2 Comparison between our LULC data and seven mainstream LULC products in 2020

The overall accuracy of our LULC data in 2020 was noticeably higher than that of the mainstream LULC products, surpassing 0.900, and the user accuracy and producer accuracy for each LULC type were also relatively high (Table S2). For the mainstream LULC products, the overall accuracy of ESA_LC was relatively high, reaching 0.697, whereas the overall accuracy of ESRI_LC was the lowest at 0.345. From the perspective of user accuracy and producer accuracy, all datasets had relatively high precision in differentiating unused land and water body. The accuracy was relatively low for cropland and construction land, which is primarily due to the relatively lower level of product refinement. The accuracy of ESA_LC and Globalland30 for woodland was relatively high, demonstrating the products' sensitivity to LULC types with vegetation cover.

Additionally, a detailed analysis of the LULC classification performance was conducted in five typical regions for primary LULC types (Fig. 3). The LULC data in this study demonstrated good boundary consistency, and was able to accurately distinguish between cropland and construction land and reasonably identify woodland and grassland. Additionally, it provided clear delineation of the boundaries of water body. In contrast, the classification performance of ESRI_LC was

significantly deficient; the dataset was almost unable to differentiate between woodland and grassland, and also misclassified large areas of land as unused land.

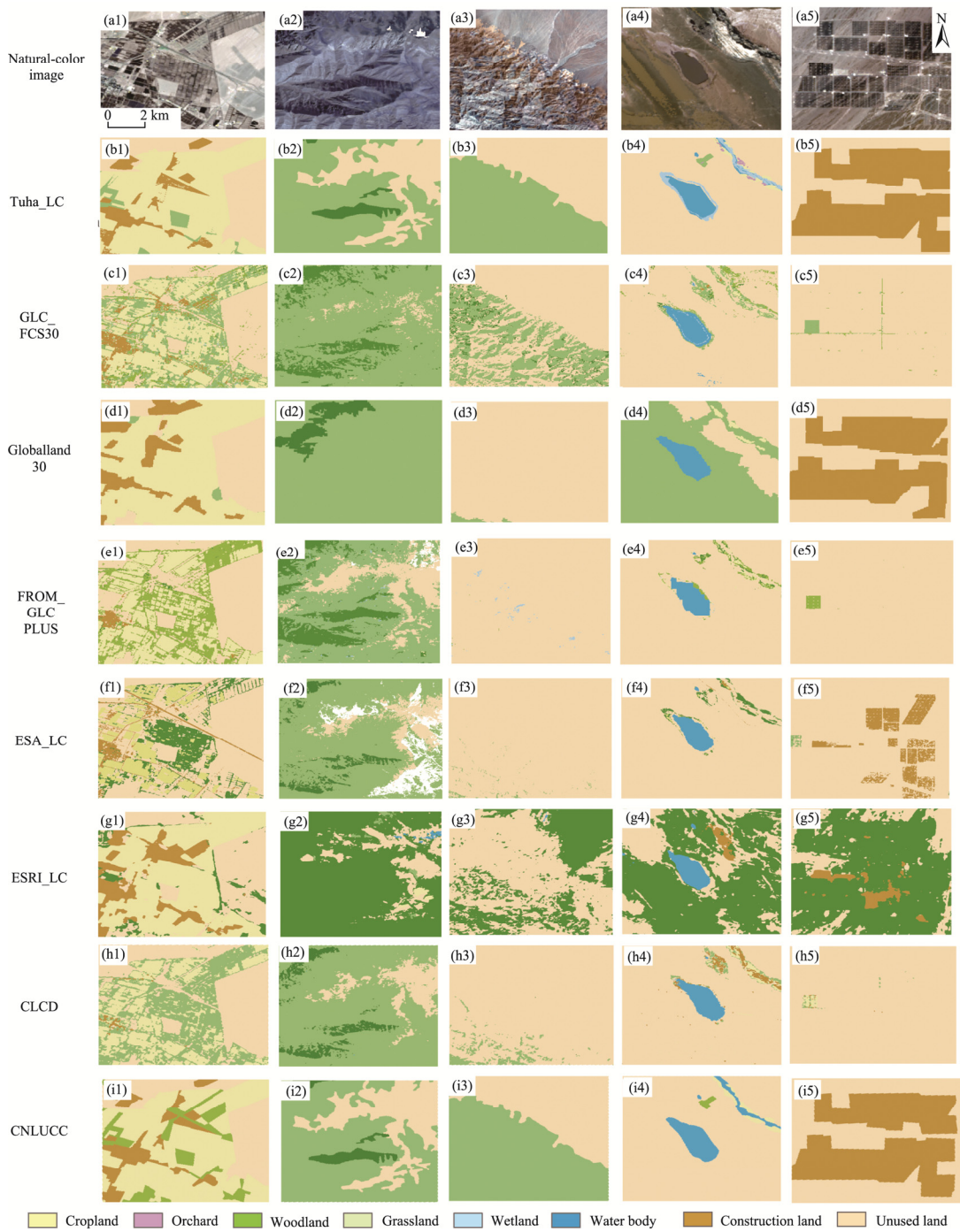


**Fig. 3** Comparison of LULC classification performance between our LULC data and seven mainstream LULC products for primary LULC types in 2020 in five typical regions. (a1–a5), natural-color images created using bands 4, 3, and 2 from Landsat 8 data in 2020; (b1–b5), Tuha_LC; (c1–c5), GLC_FCS30; (d1–d5), Globelland30; (e1–e5), FROM_GLC PLUS; (f1–f5), ESA_LC; (g1–g5), ESRI_LC; (h1–h5), CLCD; (i1–i5), CNLUCC. Tuha_LC represents our LULC data. GLC_FCS30, Global 30-meter Land Cover with Fine Classification System; FROM_GLC PLUS, Finer Resolution Observation and Monitoring of Global Land Cover PLUS; ESA_LC, ESA Global Land Cover; ESRI_LC, Esri Land Cover; CLCD, China Annual Land Cover Dataset; CNLUCC, China Multi-Period Land Use Land Cover Change Remote Sensing Monitoring Dataset.

### 4.2 Spatiotemporal evolution analysis of LULC in the Tuha Basin

#### 4.2.1 LULC evolution in the Tuha Basin from 1990 to 2020

Figure 4 shows the spatial distribution of LULC in the Tuha Basin spanning the period of 1990–2020. In 2020, unused land represented the highest proportion of 78.0%, followed by grassland, with proportion of 18.6%. All other LULC types accounted for relatively small proportions, each contributing less than 1.0% of the total land coverage; however, they have borne a significant development burden in the basin. Unused lands were located primarily south of the Bogda Peak and north of the Moqinwula Mountains, which are the eastern extensions of the Tianshan Mountains. Woodlands and grasslands mainly extended along the mountain ranges. Croplands and orchards were partially concentrated in the oasis regions of the basin; they formed contiguous patterns along the sides of the Huoyan Mountain in Turpan City, and chiefly distributed across the oasis south of the Barkol Mountains and the oasis situated between the foothills of the Tianshan Mountains and Barkol Mountains in Hami City. Water bodies and wetlands were predominantly found in the Barkol Mountains. In terms of construction land, urban and rural residential areas were mostly distributed along oases, whereas industrial lands as well as wind power and photovoltaic lands were located in Gobi and desert areas.

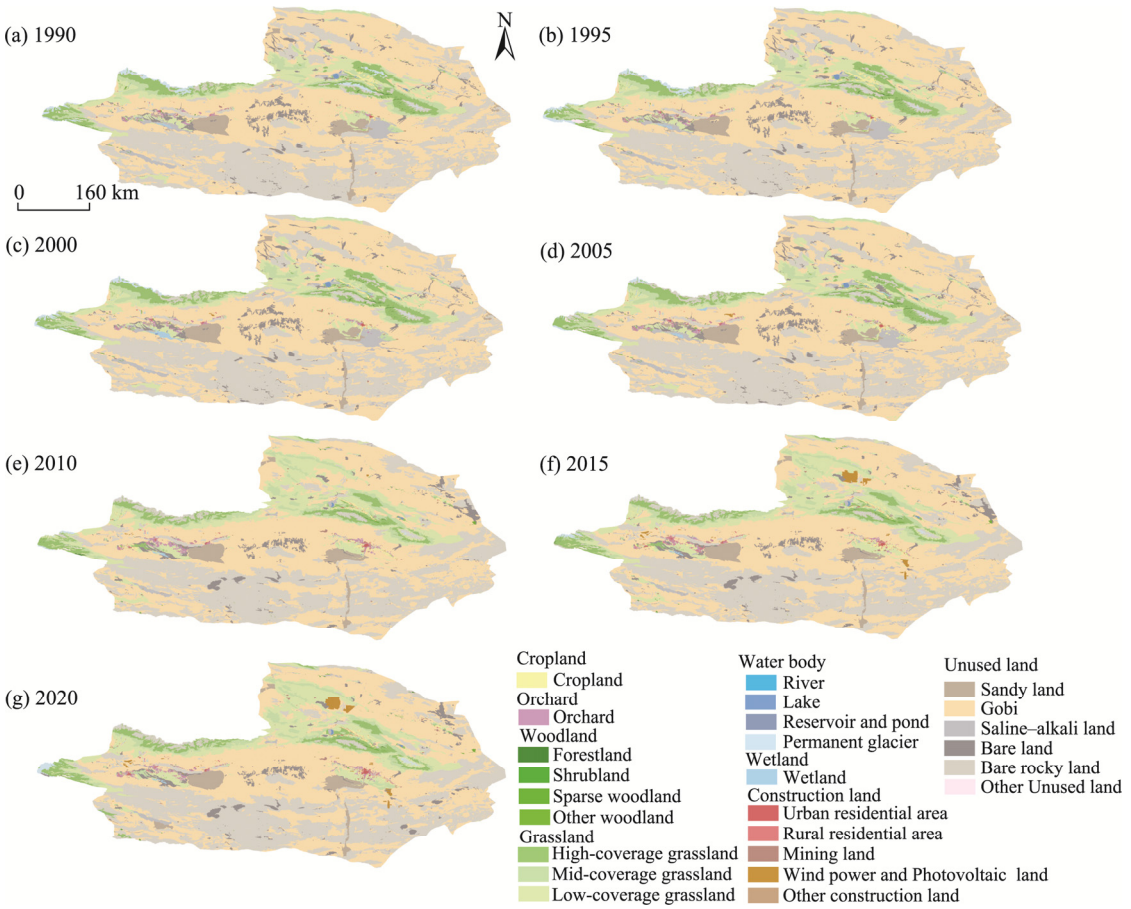


**Fig. 4** Spatial distribution of LULC in the Tuha Basin in 1990 (a), 1995 (b), 2000 (c), 2005 (d), 2010 (e), 2015 (f), and 2020 (g)

Over the past three decades, the vaiation characteristics of the primary LULC types in the Tuha Basin exhibited diverse trends (Fig. 5). During this period, the area of cropland clearly, albeit gradually, increased from 1346.49 $km^2$ in 1990 to 2473.68 $km^2$ in 2020. Orchard area generally increased from 784.83 $km^2$ in 1990 to 1022.48 $km^2$ in 2020, with a significant spike between

2000 and 2005. Conversely, the change in woodland area was relatively minor, decreasing slightly from 893.07 km$^2$ in 1990 to 685.40 km$^2$ in 2020, whereas grassland area experienced rapid expansion between 2005 and 2010, from 33,778.56 to 40,913.60 km$^2$. The fluctuations in wetland and water body were minimal. The area of water body dramatically decreased from 1903.53 km$^2$ in 1990 to 746.81 km$^2$ in 2020. Nonetheless, during the period of 2015–2020, the area of water body increased sharply, mainly in reservoir and pond. Moreover, the area of construction land expanded considerably from 270.30 km$^2$ in 1990 to 2132.86 km$^2$ in 2020, coinciding with a significant reduction in unused land from 182,342.21 km$^2$ in 1990 to 172,883.30 km$^2$ in 2020, particularly between 2005 and 2010. From the perspective of secondary LULC types

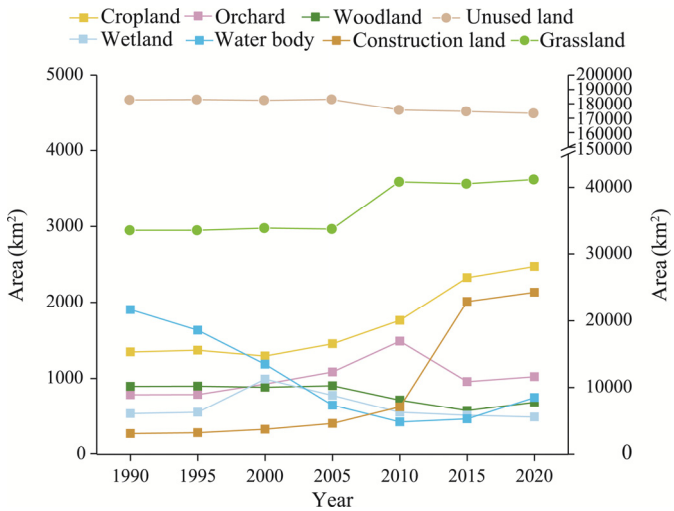


**Fig. 5** Temporal variation in area of each primary LULC type in the Tuha Basin from 1990 to 2020. Note that grassland and unused land are represented on the right-hand axis, while other LULC types correspond to the left-hand axis.

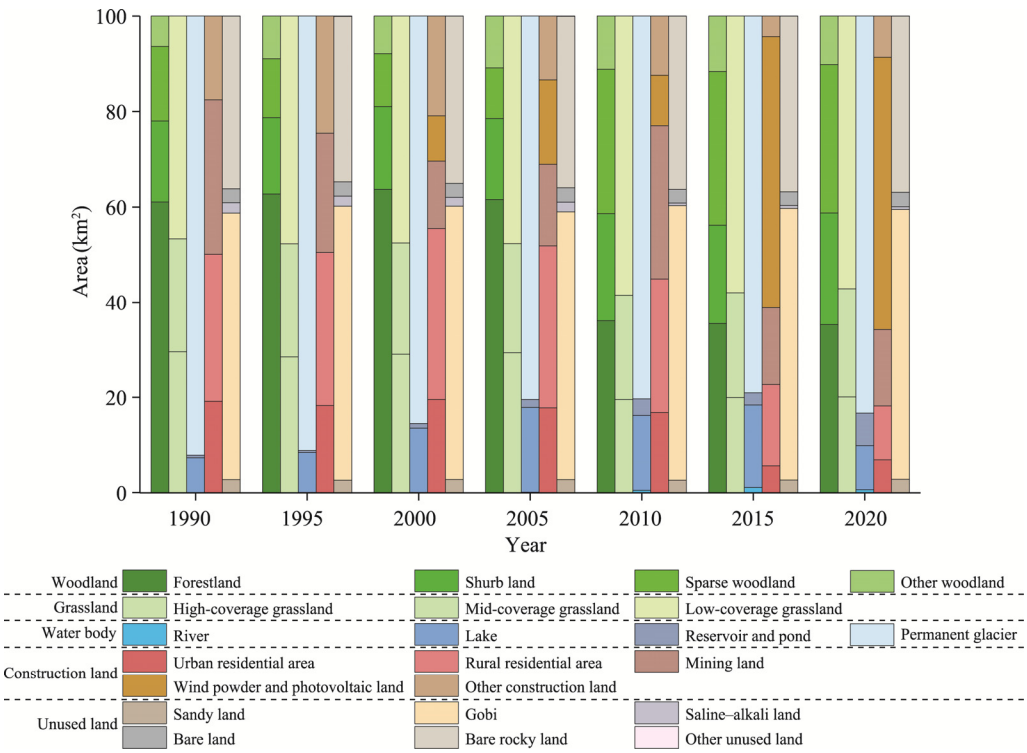


**Fig. 6** Temporal variation in area of each secondary LULC type in the Tuha Basin from 1990 to 2020

(Fig. 6), the proportion of forestland was the highest within the primary LULC type of woodland, and the presence of sparse woodland noticeably increased during 1990–2020. For grassland, areas with high coverage significantly decreased, whereas other grasslands generally showed increasing trends. With respect to water body, permanent glacier constituted the largest share, and there was a substantial increase in areas of pond, reservoir, and permanent glacier from 2015 to 2020. In terms of construction land, the area of mining land displayed a continuous growth pattern, while area of wind power and photovoltaic land started to rise after 2000, peaking in 2015. Unused lands were predominantly Gobi, whose share remained relatively stable.

In terms of dynamic degree, water body exhibited fluctuating trends and notably increased by 14.6% from 2015 to 2020 (Fig. 7). The area of construction land continued to increase, with a significant increase observed from 2010 to 2015 and a dynamic degree of 27.3%. In the initial three periods (1990–1995, 1995–2000, and 2000–2005), the comprehensive dynamic degree displayed marginal fluctuations, ranging from 0.3% to 1.0%. However, notable escalation was discerned during 2005–2010, marked by a comprehensive dynamic degree of 7.3%, signifying a consequential shift in LULC patterns. Successive periods of 2010–2015 and 2015–2020 exhibited comparatively subdued comprehensive dynamic degree of 1.9% and 1.2%, respectively, implying a stabilization or reduction in the magnitude of LULC changes.

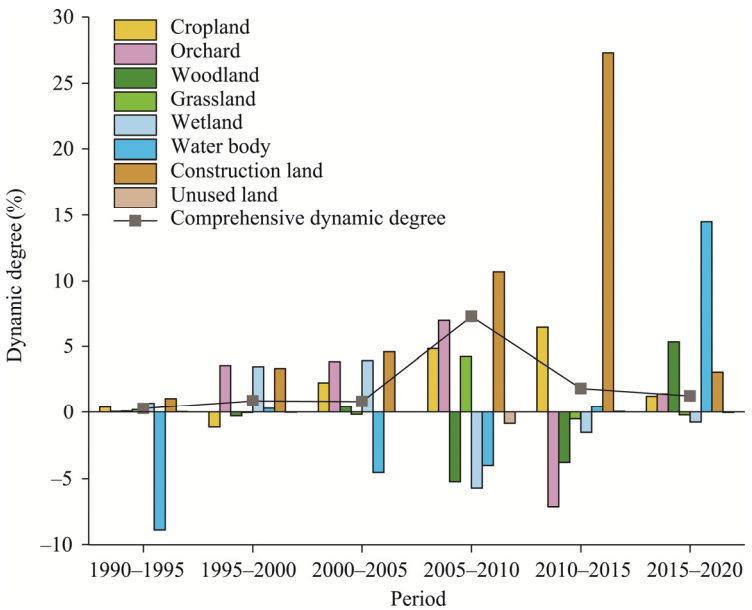


**Fig. 7** Variation in single dynamic degree and comprehensive dynamic degree of LULC in the Tuha Basin in different periods from 1990 to 2020

### 4.2.2 Transitions between primary LULC types in the Tuha Basin from 1990 to 2020

Figure 8 presents a Sankey diagram illustrating the transitions of LULC in the Tuha Basin in different periods from 1990 to 2020. The LULC transitions exhibited marked stability in different periods. Conversion from unused land to grassland was quite prominent, with the transition area reaching 12,562.41 $km^2$ between 2005 and 2010 and 2328.14 $km^2$ between 2015 and 2020 (Table S3). Such transitions are associated with national initiatives aimed at combating desertification and integrating land development for ecological restoration. Unused land also exhibited large conversions to other LULC types. From 2010 to 2015, 1295.40 $km^2$ of unused land was converted to construction land, driven by urban expansion due to economic growth and increased population. From 1990 to 1995, water body primarily transitioned to unused land, with a shift of 532.84 $km^2$, and from 1995 to 2000, another 340.75 $km^2$ of water body underwent a similar transition. Grassland experienced notable changes as well. Between 2005 and 2010, 5390.03 $km^2$ of grassland was converted to unused land, whereas between 1995 and 2000, 330.82 $km^2$ of

cropland was converted to grassland. Additionally, from 2010 to 2015, 379.42 km$^2$ of grassland was transformed into woodland, reflecting ongoing ecological restoration efforts. Construction land showed continuous growth, with significant increases observed in all periods. From 2015 to 2020, construction land increased to 1604.39 km$^2$, underscoring the rapid urbanization and development in the region. The transitions also included minor but noteworthy changes, such as the conversion of grassland to cropland, with a transition area of 349.29 km$^2$ between 2005 and 2010, and grassland to water body, with a transition area of 282.08 km$^2$ from 2015 to 2020. Wetland transitions were less prominent but still significant, with 370.63 km$^2$ of unused land converted to wetland between 1995 and 2000. Overall, these detailed transition data provide a comprehensive understanding of LULC changes within the Tuha Basin, highlighting the influence of national policies and socio-economic factors.

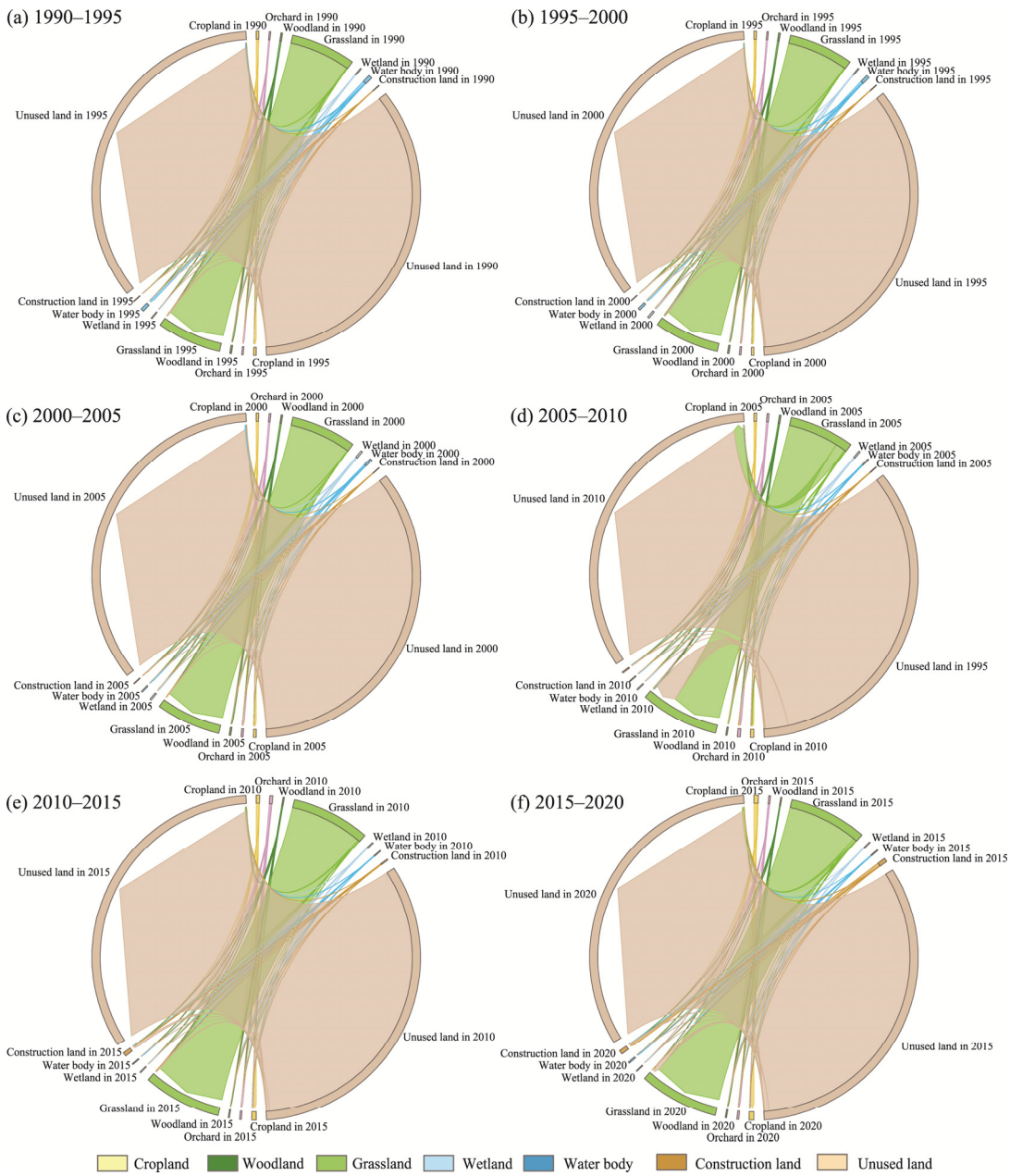


**Fig. 8** Sankey diagram illustrating the transitions between primary LULC types in the Tuha Basin during the periods of 1990–1995 (a), 1995–2000 (b), 2000–2005 (c), 2005–2010 (d), 2010–2015 (e), and 2015–2020 (f)

### 4.3 Scenario simulation and analysis of future LULC in the Tuha Basin

The Markov-FLUS model demonstrated its feasibility, with an RMSE of 0.087, indicating a good fit for the ANN model in simulating land suitability probabilities. Furthermore, the simulation of LULC data in 2020 based on LULC data in 2010 achieved a kappa coefficient of 0.859 and an overall accuracy of 0.947. These metrics collectively affirmed the model's robustness and suitability for simulating future land use scenarios in the Tuha Basin.

Under the business-as-usual scenario, it was estimated that by 2030, the area of cropland will continue to increase, whereas the area of orchard will slightly decrease, indicating an overall expansion trend in agricultural land use (Table 3). Woodland area will experience a slight reduction, with changes not exceeding 10.00 $km^2$, whereas grassland area is expected to grow, reaching as much as 42,306.87 $km^2$ by 2050. Wetland area is anticipated to continue to decline, decreasing from 447.04 $km^2$ in 2030 to 358.48 $km^2$ in 2050, indicating a need for attention toward wetland conservation and restoration. The area of water body is expected to expand in the future, while the area of construction land is expected to rapidly expand from 2886.44 $km^2$ in 2030 to 4290.44 $km^2$ by 2050, driven primarily by the conversion of unused land. Despite the vast extent of unused land, it remains relatively stable, as the conversion to construction land has not been substantial enough to significantly impact its overall extent. Under the economic development scenario, compared with that under the business-as-usual scenario, the growth of cropland is somewhat slower, reaching only 3018.36 $km^2$ by 2050, and the decrease in orchard area is more pronounced. The increase in woodland area will slightly decelerate, stabilizing at 726.46 $km^2$ by 2050, whereas the grassland area will undergo a significant decrease, reflecting changes in land use structure and increasing pressure on ecosystems. The decline in wetland area is even more drastic, falling to 326.26 $km^2$ by 2050. Similarly, the area of water body will continue to rise, reaching 1234.33 $km^2$ in 2050. The expansion of construction land is more distinct, increasing to 7130.56 $km^2$ by 2050, suggesting that under the influence of economic development, the rates of urbanization and industrial land expansion are accelerating. The reduction in unused land area is more noticeable, revealing a trend of more unused land being transformed into construction land.

**Table 3** Simulated area of each primary LULC type in the Tuha Basin under the business-as-usual and economic development scenarios in 2030, 2040, and 2050

| Scenario | Year | Area ($km^2$) | | | | | | | |
|---|---|---|---|---|---|---|---|---|---|
| | | Cropland | Orchard | Woodland | Grassland | Wetland | Water body | Construction land | Unused land |
| Business-as-usual scenario | 2030 | 2924.26 | 877.05 | 697.77 | 41,590.16 | 447.04 | 971.22 | 2886.44 | 171,325.79 |
| | 2040 | 3326.94 | 767.46 | 694.54 | 41,948.26 | 400.11 | 1130.06 | 3596.53 | 169,855.80 |
| | 2050 | 3697.84 | 678.18 | 691.28 | 42,306.87 | 358.48 | 1274.75 | 4290.44 | 168,421.88 |
| Economic development scenario | 2030 | 2864.47 | 872.64 | 701.90 | 39,740.00 | 425.18 | 958.00 | 2964.71 | 173,192.83 |
| | 2040 | 3052.29 | 777.79 | 714.74 | 38,207.60 | 368.84 | 1169.38 | 4707.38 | 172,721.68 |
| | 2050 | 3018.36 | 755.14 | 726.46 | 36,427.31 | 326.26 | 1234.33 | 7130.56 | 172,101.31 |

The distribution patterns of LULC in the Tuha Basin displayed distinctive spatial differences across different scenarios (Fig. 9). In contrast to natural expansion, the construction land expansion is more pronounced under the economic development scenario. The construction land area in regions A, B, and C has shown a significant growth tendency. However, even though the expansion of construction land area in the region A of Turpan City is evident, its growth pace is relatively slower than that of the region B in Hami City. Most notably, regions B and C will experience the most significant increase in area of construction land in Hami City. More specifically, the expansion of construction land in the region B of Barkol Kazakh Autonomous County primarily stems from the conversion of unused land and grassland. In the region C, LULC change is chiefly characterized by the transition of cropland and unused land for construction development purposes.

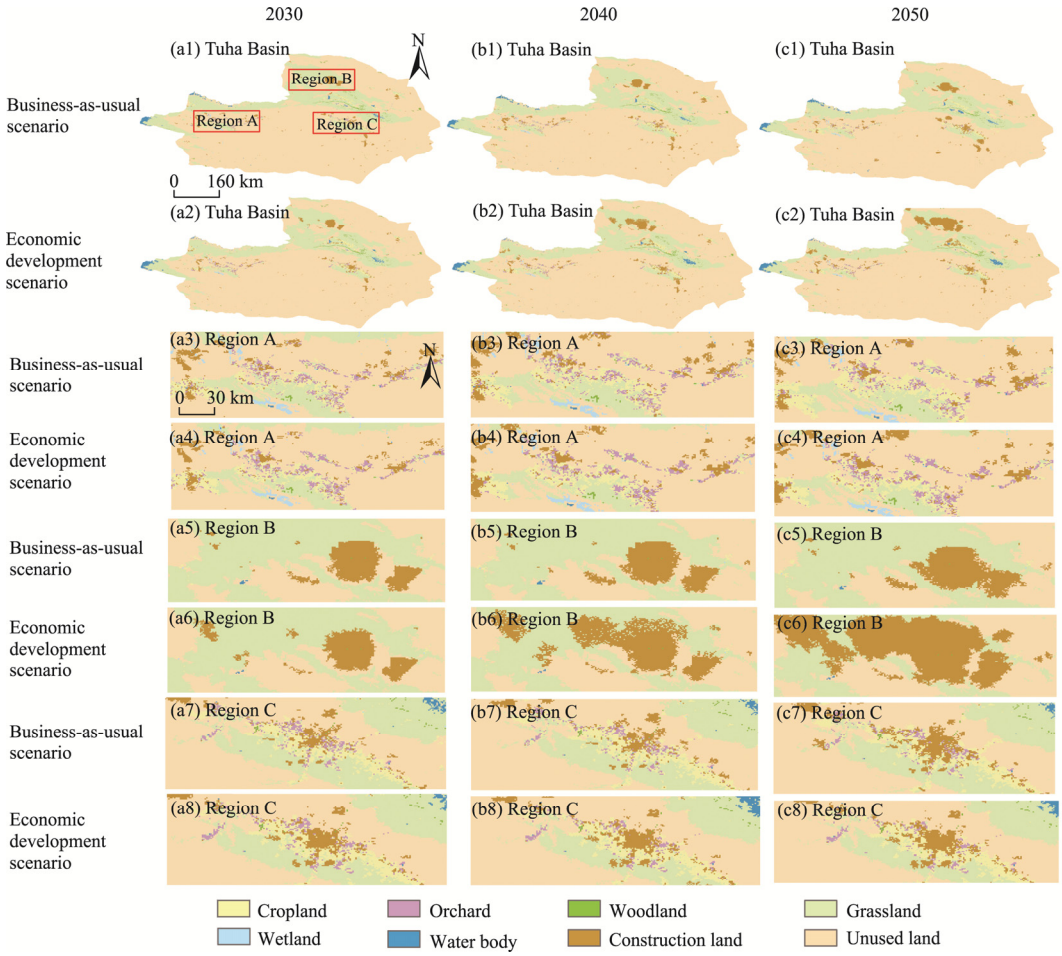


**Fig. 9** Spatial distribution of simulated LULC in the Tuha Basin and three partial regions under the business-as-usual and economic development scenarios in 2030 (a1–a8), 2040 (b1–b8), and 2050 (c1–c8)

## 5 Discussion

LULC classification in arid areas has evolved from traditional pixel-based classification and object-oriented techniques to the application of artificial intelligence algorithms such as machine learning and deep learning (Yan and Chen, 2003; Halmy and Gessler, 2015; Luo et al., 2021). However, current LULC products are primarily at global and national scales, rendering them partially inapplicable to the specific context of the local scale, such as the Tuha Basin, due to an incomplete adaptation of classification systems (Du et al., 2023). Additionally, there is a lack of refinement into secondary LULC types based on natural properties, land cover features, and land use. Our study formulated a bespoke secondary classification system for the Tuha Basin through manual interpretation. For example, woodland was further subdivided into forestland, shrub land, sparse woodland, and other woodland types, which allows for an in-depth understanding of specific ecological characteristics. For water body, the secondary types of river, lake, reservoir, and pond were set to distinguish natural water bodies from artificially constructed water bodies. Simultaneously, permanent glacier was established to understand the status of glacier changes in this basin. For construction land, specially designed secondary LULC types such as mining land and wind power and photovoltaic land were identified to aid analyses pertinent to adjustments in the energy structure. Our targeted approach significantly improved the classification accuracy, with an average overall accuracy of 0.917 for the primary LULC types and 0.864 for the secondary LULC types. Compared with the mainstream LULC products, the accuracy of our main

primary LULC types was improved by more than 20.0%. Moreover, the producer accuracy and user accuracy for cropland, woodland, and construction land increased by more than 40.0%. This addressed the limits of the automated data classification system in distinguishing between woodland and grassland or between cropland and orchard. At present, large-scale and long-term studies of LULC in the Tuha Basin are relatively scarce, and data are somewhat lacking compared with those in other regions (Liu et al., 2023). This high-precision secondary classification of LULC data provides reliable information for research regarding the ecologically, environmentally, and socially sustainable development of the Tuha Basin. However, our method has several limitations. In the Tuha Basin, where the LULC is complex and a secondary classification system is needed, we chose manual interpretation to implement LULC classification. First, while manual interpretation can provide high accuracy, it requires significant labor and time that are not scalable for larger areas or extended time frames. Future improvements could increase the precision of LULC classification by incorporating more detailed data sources, such as high-resolution remote sensing imagery, multitemporal datasets, and phenological data. Second, LULC change is a complex and dynamic process with considerable uncertainty. The model parameters in this study, such as neighborhood factors, were primarily based on previous research and the extent of human impact on different LULC types, introducing a degree of subjectivity. In this study, our scenario simulations included only primary LULC types, and further refinement into secondary LULC types could be explored. Nonetheless, our research offers a robust and precise data foundation that is essential for land use management and policy formulation at the local scale in the Tuha Basin.

Owing to the arid climate and scarcity of water resources in arid areas, much of the land remains unutilized. Arable land is relatively rare and predominantly concentrated in river basins or oasis areas, relying heavily on irrigated agriculture, which makes water resources crucial for development (Zhou et al., 2008; Chen et al., 2022a). The Tuha Basin exemplifies these characteristics, with unused land being the predominant LULC type from 1990 to 2020, followed by grassland. In agricultural terms, croplands and orchards that primarily located in oasis areas are central to the region's agricultural production. Despite the constraints of arid environment, croplands and orchards have expanded significantly, growing by approximately 1364.83 $km^2$ from 2131.32 $km^2$ in 1990 to 3496.15 $km^2$ in 2020, demonstrating the region's strategic adaptability to its conditions. In terms of water resources, there has been a notable reduction in the spatial extent of water bodies, which are essential for sustaining and developing arid areas. This trend requires increased attention. However, since 2015, there has been significant growth in the area of reservoir and pond, reflecting the profound impact of human activities on water resource management. This expansion is closely linked to the "red line" policy implemented by the Chinese State Council, which aims to ensure sustainable water resource utilization within Xinjiang. The policy focuses on controlling water resource development, enhancing efficiency, and reducing pollution in water functional zones, leading to observed growth in reservoir and pond (Chen et al., 2020b). From the perspective of energy structure, the area of mining land steadily increased, whereas land designated for wind power and photovoltaic use expanded by more than 1000.00 $km^2$ between 2010 and 2015. This reflects a trend in energy development, shifting the focus toward new, clean energy sources and aligning with energy development policies (Deng et al., 2022). Ecological sustainability remains a critical issue, as evidenced by the reduction in areas of grassland and wetland from 2005 to 2010. This decline highlights the need for sustainable development strategies focused on ecological conservation, as these diminishing areas are likely to result from increased human activities.

Future simulation of LULC not only exposed the ecological protection challenges faced by the Tuha Basin but also highlighted the necessity of parallel socio-economic and ecological development. Under the business-as-usual scenario, the areas of cropland and construction land are projected to expand continuously, whereas the significant decreases in grassland and wetland areas highlight the urgency of ecological preservation. Under the economic development scenario,

the rapid expansion of construction land, primarily through the conversion of unused land, highlights the development potential of unused land. Thus, to achieve sustainable development, it is vital to balance the needs of economic growth and environmental protection, considering both short-term economic gains and long-term ecological benefits (Wang et al., 2021). The current ecological protection policy in the Tuha Basin mainly favors integrated management of mountains, water, forests, fields, lakes, grasses, and sands, and fully considers the contribution of the systems of rivers, lakes, forests, and grasses to human health, focusing on the protection of water (Kou et al., 2024; Toops, 2015). There is a pressing need for government authorities and decision makers to strengthen the conservation of fragile ecosystems such as wetlands and grasslands, ensuring rational water use and the preservation of soil-related environmental functions. Local governments should fully tap into its unused potential, implement sustainable land planning and management, pay close attention to water resource management, continue to promote the transformation of the energy structure, and achieve a balance between economic growth, urban development, and ecological protection.

## 6 Conclusions

This study established a 30-m resolution LULC classification dataset with high accuracy in the Tuha Basin from 1990 to 2020. The results revealed that the primary LULC types had an average overall accuracy of 0.917 and the secondary LULC types had an average overall accuracy of 0.864. In the Tuha Basin, unused land consistently occupied the largest share in terms of area, averaging above 70.0%, followed by grassland. Despite comprising less than 1.0% of the total area, cropland and construction land played pivotal roles in arid land development and were expanding rapidly. These lands were predominantly located within oases that form the urban core of the Turpan City and Hami City. Water body, which is important for the development of the region, experienced a decline in total area, resulting in a resurgence after 2015 due to increased reservoir and pond areas. Land transitions in the Tuha Basin demonstrated relative stability in different periods from 1990 to 2020. The development of the region should fully tap into the potential of unused land while continuing to focus on water resource management. The LULC simulations revealed that under the business-as-usual scenario, both cropland and construction land will increase, whereas wetland will decrease, emphasizing the need for ecological conservation. Under the economic development scenario, urbanization and industrial land expansion are more pronounced, with slower cropland growth and greater reductions in grassland and wetland. These findings highlight the need for balanced regional planning to achieve sustainable land use. Furthermore, the development and shifts in land use within the basin are asymmetric across different regions, necessitating a more granular approach to regional planning and policy drafting.

## Conflict of interest

The authors declare that they have no known competing financial interests or personal relationships that could have appeared to influence the work reported in this paper.

## Acknowledgements

This work was supported by the Third Xinjiang Scientific Expedition Program (2022xjkk1100) and the Tianchi Talent Project.

## Author contributions

Data Curation: CHEN Yiyang, DONG Yuqi, SHAO Wei, ZHANG Qinglan; Methodology: CHEN Yiyang; Software: CHEN Yiyang; Formal analysis: CHEN Yiyang; Writing - original draft: CHEN Yiyang; Visualization validation: CHEN Yiyang; Conceptualization: ZHANG Li, YAN Min, WU Yin; Writing - review & editing:

ZHANG Li, YAN Min, WU Yin; Resources: ZHANG Li; Supervision: ZHANG Li; Project administration: ZHANG Li; Funding acquisition: ZHANG Li; Investigation: DONG Yuqi, SHAO Wei, ZHANG Qinglan. All authors approved the manuscript.

## References

Alijani Z, Hosseinali F, Biswas A. 2020. Spatio-temporal evolution of agricultural land use change drivers: A case study from Chalous region, Iran. Journal of Environmental Management, 262: 110326, doi: 10.1016/j.jenvman.2020.110326.

Bi W X, Weng B S, Yuan Z, et al. 2018. Evolution characteristics of surface water quality due to climate change and LUCC under scenario simulations: A case study in the Luanhe River Basin. International Journal of Environmental Research and Public Health, 15(8): 1724, doi: 10.3390/ijerph15081724.

Chen C, He X Y, Liu Z S, et al. 2020a. Analysis of regional economic development based on land use and land cover change information derived from Landsat imagery. Scientific Reports, 10(1): 12721, doi: 10.1038/s41598-020-69716-2.

Chen H S, Li X, Hua W J. 2015a. Numerical simulation of the impact of land use/land cover change over China on regional climates during the last 20 years. Chinese Journal of Atmospheric Sciences, 39(2): 357–369. (in Chinese)

Chen J, Chen J, Liao A P, et al. 2015b. Global land cover mapping at 30m resolution: A POK-based operational approach. ISPRS Journal of Photogrammetry and Remote Sensing, 103: 7–27.

Chen J Q, John R, Yuan J, et al. 2022a. Sustainability challenges for the social-environmental systems across the Asian Drylands Belt. Environmental Research Letters, 17(2): 023001, doi: 10.1088/1748-9326/ac472f.

Chen L T, Cai H S, Zhang T, et al. 2022b. Land use multi-scenario simulation analysis of Rao River Basin based on Markov-FLUS model. Acta Ecologica Sinica, 42(10): 3947–3958. (in Chinese)

Chen X, Cun C, Bao A M, et al. 2020b. Spatial pattern and characteristics of land cover change in Xinjiang since past 40 years of the economic reform and opening up. Arid Land Geography, 43(1): 1–11. (in Chinese)

Chen Y M, Li X, Liu X P, et al. 2016. Capturing the varying effects of driving forces over time for the simulation of urban growth by using survival analysis and cellular automata. Landscape and Urban Planning, 152: 59–71.

Deng M J, Ming B, Li Y, et al. 2022. Pathways towards a cleaner energy system for Xinjiang under carbon peak and carbon neutrality goals. Journal of Natural Resources, 37(5): 1107–1122. (in Chinese)

Dong X B, Liu M X. 2022. Relationships among LUCC, ecosystem services and human well-being. Journal of Beijing Normal University (Natural Science), 58(3): 465–475. (in Chinese)

Du H Y, Zhou C, Tang H Q, et al. 2021. Simulation and estimation of future precipitation changes in arid regions: A case study of Xinjiang, Northwest China. Climatic Change, 167: 43, doi: 10.1007/s10584-021-03192-z.

Du H Y, Li M C, Xu Y Y, et al. 2023. An ensemble learning approach for land use/land cover classification of arid regions for climate simulation: A case study of Xinjiang, northwest China. IEEE Journal of Selected Topics in Applied Earth Observations and Remote Sensing, 16: 2413–2426.

Gharbia S S, Alfatah S A, Gill L, et al. 2016. Land use scenarios and projections simulation using an integrated GIS cellular automata algorithms. Modeling Earth Systems and Environment, 2(3): 151, doi: 10.1007/s40808-016-0210-y.

Gómez C, White J C, Wulder M A. 2016. Optical remotely sensed time series data for land cover classification: A review. ISPRS Journal of Photogrammetry and Remote Sensing, 116: 55–72.

Halmy M W A, Gessler P E. 2015. The application of ensemble techniques for land-cover classification in arid lands. International Journal of Remote Sensing, 36(22): 5613–5636.

He C Y, Zhang J X, Liu Z F, et al. 2022. Characteristics and progress of land use/cover change research during 1990–2018. Journal of Geographical Sciences, 32(3): 537–559. (in Chinese)

Hu S, Chen L Q, Li L, et al. 2020. Simulation of land use change and ecosystem service value dynamics under ecological constraints in Anhui Province, China. International Journal of Environmental Research and Public Health, 17(12): 4228, doi: 10.3390/ijerph17124228.

Karra K, Kontgis C, Statman-Weil Z, et al. 2021. Global land use/land cover with Sentinel 2 and deep learning. 2021 Institute of Electrical and Electronics Engineers (IEEE) International Geoscience and Remote Sensing Symposium (IGARSS). Brussels: IEEE, 4704–4707.

Kou Y F, Chen S M, Zhou K F, et al. 2024. Spatiotemporal patterns and coupling coordination analysis of multiscale social–economic–ecological effects in ecologically vulnerable areas based on multi-source data: A case study of the Tuha Region, Xinjiang Province. Land, 13(3): 282, doi: 10.3390/land13030282.

Kuang W H, Zhang S W, Du G M, et al. 2022. Remotely sensed mapping and analysis of spatio-temporal patterns of land use change across China in 2015–2020. Acta Geographics Sinica, 77(5): 1056–1071. (in Chinese)

Li C J, Fu B J, Wang S, et al. 2021. Drivers and impacts of changes in China's drylands. Nature Reviews Earth & Environment,

2(12): 858–873.

Li X, Zhang J C, Gao H S, et al. 2024. Spatiotemporal variation characteristics of ecosystem carbon storage in Henan Province and future multi-scenario simulation prediction. Land, 13(2): 185, doi: 10.3390/land13020185.

Liu J Y, Zhang Z X, Xu X L, et al. 2010. Spatial patterns and driving forces of land use change in China during the early 21st century. Journal of Geographical Sciences, 20(4): 483–494. (in Chinese)

Liu S, Xu Z L, Guo Y C, et al. 2023. Consistency analysis of multi-source remote sensing land cover products in arid regions—A case study of Xinjiang. Land, 12(12): 2178, doi: 10.3390/land12122178.

Liu X P, Liang X, Li X, et al. 2017. A future land use simulation model (FLUS) for simulating multiple land use scenarios by coupling human and natural effects. Landscape and Urban Planning, 168: 94–116.

Luo J C, Hu X D, Wu T J, et al. 2021. Research on intelligent calculation model and method of precision land use/cover change information driven by high-resolution remote sensing. National Remote Sensing Bulletin, 25(7): 1351–1373. (in Chinese)

Luo K S, Zhang X J. 2022. Increasing urban flood risk in China over recent 40 years induced by LUCC. Landscape and Urban Planning, 219: 104317, doi: 10.1016/j.landurbplan.2021.104317.

Olofsson P, Giles M F, Stehman S V, et al. 2013. Making better use of accuracy data in land change studies: Estimating accuracy and area and quantifying uncertainty using stratified estimation. Remote Sensing of Environment, 129(12): 122–131.

Özşahin E, Eroğlu I. 2019. Soil erosion risk assessment due to land use/cover changes (LUCC) in Bulgaria from 1990 to 2015. Alinteri Journal of Agriculture Science, 34(1): 1–8.

Ren Q, He C Y, Huang Q X, et al. 2022. Impacts of urban expansion on natural habitats in global drylands. Nature Sustainability, 5(10): 869–878.

Schirpke U, Tscholl S, Tasser E. 2020. Spatio-temporal changes in ecosystem service values: Effects of land-use changes from past to future (860–2100). Journal of Environmental Management, 272: 111068, doi: 10.1016/j.jenvman.2020.111068.

Shan X M, Yin J, Wang J. 2022. Risk assessment of shanghai extreme flooding under the land use change scenario. Natural Hazards, 110(2): 1039–1060.

Toops W S. 2015. The ecology of Xinjiang: a focus on water. In: Frederick Starr S. Xinjiang. New York: Routledge, 264–275.

Wang H, Liu Y X, Wang Y J, et al. 2023. Land cover change in global drylands: A review. Science of the Total Environment, 863(1): 160943, doi: 10.1016/j.scitotenv.2022.160943.

Wang K B, Deng L, Shangguan Z P, et al. 2021. Sustainability of eco-environment in semi-arid regions: Lessons from the Chinese Loess Plateau. Environmental Science & Policy, 125: 126–134.

Wang Y J, Wu S F. 2003. Environment change over the Aydingkol Lake Region in the Turpan Basin, Xinjiang. Journal of Glaciology and Geocryology, 25(2): 229–231. (in Chinese)

Xu C G, McDowell N G, Fisher R A, et al. 2019. Increasing impacts of extreme droughts on vegetation productivity under climate change. Nature Climate Change, 9(12): 948–953.

Xu X L, Liu J Y, Zhang S W, et al. 2018. China's Multi-Period Land Use Land Cover Remote Sensing Monitoring Dataset (CNLUCC). Beijing: Data Registration and Publishing System of the Resource and Environmental Science Data Center of the Chinese Academy of Sciences.

Yan J F, Chen X. 2003. Analysis and stimulation method discussion on LUCC of arid region based on GIS. Arid Land Geography, 26(2): 185–191. (in Chinese)

Yang J, Huang X. 2021. 30 m annual land cover and its dynamics in China from 1990 to 2019. Earth System Science Data Discussions, 13(8): 2907–2925.

Yang M, Zhang G L, Hou Y P. 2011. Advances and prospects of the driving force of regional land use change researches. Geography and Geo-Information Science, 27(1): 95–100. (in Chinese)

Yimuranjiang A, Zhang Y F, Zibibula S. 2021. A study on change of land use pattern in Hami City during 2000–2020 based on GlobeLand30. Bulletin of Soil and Water Conservation, 41(1): 182–189, 196. (in Chinese)

Yu L, Du Z R, Dong R M, et al. 2022. FROM-GLC Plus: Toward near real-time and multi-resolution land cover mapping. GIScience & Remote Sensing, 59(1): 1026–1047.

Zanaga D, van de Kerchove R, de Keersmaecker W, et al. 2021. ESA WorldCover 10 m 2020 v100. Zenodo. [2024-03-28]. https://doi.org/10.5281/zenodo.5571936.

Zhang X, Liu L Y, Chen X D, et al. 2021. GLC_FCS30: Global land-cover product with fine classification system at 30 m using time-series Landsat imagery. Earth System Science Data, 13(6): 2753–2776.

Zhou Q M, Li B, Kurban A. 2008. Trajectory analysis of land cover change in arid environment of China. International Journal of Remote Sensing, 29(4): 1093–1107.

# Appendix

**Table S1** Accuracy assessment results for each primary LULC type of Tuha_LC from 1990 to 2020

| Year | Metric | Cropland | Orchard | Woodland | Grassland | Wetland | Water body | Construction land | Unused land |
|---|---|---|---|---|---|---|---|---|---|
| 1990 | PA | 0.649 | 0.903 | 0.576 | 0.883 | 0.954 | 0.982 | 0.706 | 0.958 |
| | UA | 0.897 | 0.509 | 0.810 | 0.792 | 0.883 | 0.809 | 0.857 | 0.983 |
| 1995 | PA | 0.638 | 0.897 | 0.559 | 0.861 | 0.943 | 0.944 | 0.813 | 0.952 |
| | UA | 0.923 | 0.491 | 0.733 | 0.768 | 0.872 | 0.797 | 0.765 | 0.979 |
| 2000 | PA | 0.617 | 0.976 | 0.567 | 0.860 | 0.988 | 0.983 | 0.737 | 0.958 |
| | UA | 0.985 | 0.577 | 0.756 | 0.775 | 0.876 | 0.881 | 0.875 | 0.972 |
| 2005 | PA | 0.591 | 0.974 | 0.586 | 0.897 | 0.837 | 0.978 | 0.769 | 0.963 |
| | UA | 0.974 | 0.475 | 0.791 | 0.769 | 0.928 | 0.938 | 0.800 | 0.971 |
| 2010 | PA | 0.702 | 0.900 | 0.800 | 0.825 | 0.989 | 0.917 | 0.778 | 0.967 |
| | UA | 0.890 | 0.600 | 0.698 | 0.880 | 0.918 | 0.815 | 0.946 | 0.978 |
| 2015 | PA | 0.907 | 0.778 | 0.765 | 0.834 | 0.978 | 0.921 | 0.892 | 0.960 |
| | UA | 0.824 | 0.800 | 0.765 | 0.878 | 0.897 | 0.967 | 0.851 | 0.964 |
| 2020 | PA | 0.922 | 0.957 | 0.908 | 0.832 | 0.989 | 0.979 | 0.897 | 0.974 |
| | UA | 0.870 | 0.968 | 0.814 | 0.940 | 0.979 | 0.912 | 0.853 | 0.976 |

Note: LULC, land use/land cover. Tuha_LC represents the LULC data generated in this study. PA, producer accuracy; UA, user accuracy.

**Table S2** Accuracy assessment results for each primary LULC type of Tuha_LC and the seven mainstream LULC products in 2020

| LULC data | Metric | Cropland | Woodland | Grassland | Water body | Construction land | Unused land | OA | Kappa |
|---|---|---|---|---|---|---|---|---|---|
| Tuha_LC | PA | 0.922 | 0.957 | 0.908 | 0.832 | 0.989 | 0.979 | 0.917 | 0.845 |
| | UA | 0.870 | 0.968 | 0.814 | 0.940 | 0.979 | 0.912 | | |
| GLC_FCS30 | PA | 0.060 | 0.121 | 0.288 | 0.214 | 0.000 | 0.703 | 0.553 | 0.154 |
| | UA | 0.069 | 0.129 | 0.243 | 0.095 | 0.000 | 0.805 | | |
| Global-land30 | PA | 0.128 | 0.316 | 0.360 | 0.477 | 0.056 | 0.708 | 0.585 | 0.209 |
| | UA | 0.186 | 0.138 | 0.283 | 0.221 | 0.021 | 0.822 | | |
| FROM_GLC PLUS | PA | 0.073 | 0.041 | 0.237 | 0.283 | 0.100 | 0.679 | 0.562 | 0.121 |
| | UA | 0.069 | 0.023 | 0.177 | 0.137 | 0.010 | 0.839 | | |
| ESA_LC | PA | 0.090 | 0.451 | 0.698 | 0.306 | 0.083 | 0.806 | 0.697 | 0.451 |
| | UA | 0.098 | 0.586 | 0.822 | 0.116 | 0.010 | 0.861 | | |
| ESRI_LC | PA | 0.058 | 0.051 | 0.909 | 0.222 | 0.000 | 0.772 | 0.345 | 0.086 |
| | UA | 0.069 | 0.484 | 0.042 | 0.105 | 0.000 | 0.477 | | |
| CLCD | PA | 0.074 | 0.000 | 0.290 | 0.250 | 0.000 | 0.700 | 0.561 | 0.157 |
| | UA | 0.088 | 0.000 | 0.296 | 0.116 | 0.000 | 0.814 | | |
| CNLUCC | PA | 0.210 | 0.042 | 0.270 | 0.280 | 0.041 | 0.735 | 0.577 | 0.206 |
| | UA | 0.127 | 0.034 | 0.296 | 0.147 | 0.021 | 0.828 | | |

Note: GLC_FCS30, Global 30-meter Land Cover with Fine Classification System; FROM_GLC PLUS, Finer Resolution Observation and Monitoring of Global Land Cover PLUS; ESA_LC, ESA Global Land Cover; ESRI_LC, Esri Land Cover; CLCD, China Annual Land Cover Dataset; CNLUCC, China Multi-Period Land Use Land Cover Change Remote Sensing Monitoring Dataset; OA, overall accuracy. Kappa represents the kappa coefficient.

**Table S3** Land transitions between primary LULC types in different periods from 1900 to 2020

| Land transition | Area ($km^2$) | | | | | |
|---|---|---|---|---|---|---|
| | 1900–1995 | 1995–2000 | 2000–2005 | 2005–2010 | 2010–2015 | 2015–2020 |
| Cropland to cropland | 1243.79 | 941.15 | 1126.99 | 883.64 | 1569.73 | 1871.84 |
| Cropland to orchard | 62.46 | 41.35 | 95.80 | 290.30 | 22.47 | 288.33 |
| Cropland to woodland | 4.31 | 6.85 | 2.22 | 10.46 | 0.51 | 0.62 |
| Cropland to grassland | 19.23 | 330.82 | 33.82 | 154.76 | 88.61 | 98.49 |
| Cropland to wetland | 1.04 | 5.00 | 2.00 | 0.35 | 0.45 | 0.27 |
| Cropland to water body | 0.01 | 0.24 | 0.33 | 0.20 | 1.64 | 1.61 |
| Cropland to construction land | 5.74 | 20.64 | 14.19 | 48.64 | 49.55 | 48.27 |
| Cropland to unused land | 9.65 | 24.09 | 17.39 | 66.98 | 29.89 | 16.65 |
| Orchard to cropland | 32.34 | 35.07 | 81.35 | 230.11 | 483.09 | 297.40 |
| Orchard to orchard | 704.30 | 683.40 | 813.00 | 747.67 | 885.08 | 593.86 |
| Orchard to woodland | 26.03 | 15.98 | 9.77 | 0.58 | 0.04 | 1.17 |
| Orchard to grassland | 10.40 | 24.91 | 9.52 | 47.90 | 21.32 | 33.44 |
| Orchard to wetland | 0.30 | 0.00 | 0.03 | 0.42 | 0.17 | 0.75 |
| Orchard to water body | 0.07 | 0.06 | 0.10 | 0.11 | 0.93 | 1.08 |
| Orchard to construction land | 7.99 | 16.35 | 11.06 | 38.43 | 82.97 | 18.83 |
| Orchard to unused land | 3.15 | 11.16 | 1.80 | 16.39 | 15.48 | 4.92 |
| Woodland to cropland | 35.37 | 7.52 | 1.13 | 42.78 | 8.13 | 3.66 |
| Woodland to orchard | 5.75 | 40.35 | 33.50 | 79.62 | 0.72 | 3.82 |
| Woodland to woodland | 800.97 | 803.07 | 807.78 | 216.43 | 517.37 | 492.11 |
| Woodland to grassland | 32.45 | 32.31 | 9.06 | 497.77 | 160.08 | 37.78 |
| Woodland to wetland | 0.10 | 0.49 | 27.19 | 0.62 | 0.38 | |
| woodland to water body | 0.22 | 0.09 | 0.00 | 1.12 | 0.27 | 23.46 |
| woodland to construction land | 1.51 | 3.38 | 1.16 | 4.80 | 3.45 | 1.72 |
| woodland to unused land | 16.67 | 9.57 | 3.73 | 59.38 | 21.20 | 12.06 |
| Grassland to cropland | 36.63 | 172.11 | 145.84 | 349.29 | 154.52 | 145.66 |
| Grassland to orchard | 8.47 | 95.23 | 98.02 | 150.46 | 19.47 | 50.67 |
| Grassland to woodland | 51.74 | 41.68 | 41.30 | 379.42 | 46.46 | 155.00 |
| Grassland to grassland | 32,988.39 | 32,937.56 | 33,334.00 | 27,364.77 | 39,803.95 | 38,602.64 |
| Grassland to wetland | 3.61 | 80.38 | 19.81 | 24.71 | 7.02 | 11.78 |
| Grassland to water body | 267.14 | 55.23 | 2.27 | 60.57 | 150.85 | 282.08 |
| Grassland to construction land | 5.57 | 11.95 | 4.31 | 57.41 | 59.56 | 151.86 |
| Grassland to unused land | 249.50 | 206.37 | 275.50 | 5390.03 | 667.37 | 1219.14 |
| Wetland to cropland | 0.08 | 0.12 | 0.96 | 11.21 | 0.75 | 0.69 |
| Wetland to orchard | 0.04 | 0.26 | 0.30 | 0.34 | 0.75 | 0.03 |
| Wetland to woodland | 0.30 | 0.07 | 0.76 | 4.37 | 0.00 | 0.27 |
| Wetland to grassland | 2.89 | 1.75 | 25.20 | 184.91 | 16.67 | 27.68 |
| Wetland to wetland | 516.43 | 532.83 | 622.76 | 495.31 | 495.64 | 468.58 |
| Wetland to water body | 0.18 | 8.37 | 0.03 | 1.39 | 4.37 | 7.17 |
| Wetland to construction land | 0.12 | 0.00 | 0.38 | 0.84 | 0.70 | 1.10 |
| Wetland to unused land | 13.93 | 8.53 | 339.78 | 76.71 | 33.75 | 5.91 |
| Water body to cropland | 0.24 | 0.01 | 0.34 | 0.77 | 1.51 | 1.37 |

To be continued

Continued

| Land transition | Area ($km^2$) | | | | | |
|---|---|---|---|---|---|---|
| | 1900–1995 | 1995–2000 | 2000–2005 | 2005–2010 | 2010–2015 | 2015–2020 |
| Water body to orchard | 0.09 | 0.62 | 0.04 | 0.67 | 0.20 | 0.23 |
| Water body to woodland | 0.05 | 0.05 | 0.00 | 0.06 | 0.08 | 0.41 |
| Water body to grassland | 45.63 | 232.58 | 130.06 | 78.25 | 6.03 | 93.41 |
| Water body to wetland | 0.05 | 0.66 | 10.28 | 0.18 | 0.25 | 0.35 |
| Water body to water body | 1323.25 | 1047.25 | 640.63 | 273.92 | 250.52 | 349.89 |
| Water body to construction land | 0.00 | 0.00 | 0.00 | 1.05 | 0.01 | 1.24 |
| Water body to unused land | 532.84 | 340.75 | 401.85 | 289.53 | 164.89 | 16.90 |
| Construction land to cropland | 7.01 | 9.93 | 3.20 | 19.99 | 24.99 | 89.87 |
| Construction land to orchard | 3.46 | 15.15 | 3.46 | 37.26 | 11.59 | 34.21 |
| Construction land to woodland | 3.02 | 1.46 | 0.60 | 1.02 | 0.01 | 1.15 |
| Construction land to grassland | 3.56 | 5.54 | 0.53 | 18.42 | 6.76 | 48.62 |
| Construction land to wetland | 0.02 | 0.17 | 1.51 | 0.07 | 0.01 | 0.38 |
| Construction land to water body | 0.00 | 0.00 | 0.01 | 0.02 | 0.11 | 0.60 |
| Construction land to construction land | 247.21 | 239.19 | 316.08 | 200.22 | 522.11 | 1604.39 |
| Construction land to unused land | 6.12 | 12.69 | 4.13 | 128.90 | 57.13 | 234.53 |
| Unused land to cropland | 14.66 | 126.83 | 95.51 | 225.06 | 83.37 | 62.05 |
| Unused land to orchard | 2.35 | 50.29 | 37.50 | 182.77 | 11.18 | 49.41 |
| Unused land to woodland | 10.36 | 14.37 | 40.09 | 99.26 | 10.14 | 34.64 |
| Unused land to grassland | 497.94 | 355.60 | 234.48 | 12,562.41 | 515.41 | 2328.14 |
| Unused land to wetland | 30.36 | 370.63 | 91.50 | 30.96 | 7.51 | 8.04 |
| Unused land to water body | 31.07 | 71.96 | 1.05 | 86.16 | 55.10 | 80.52 |
| Unused land to construction land | 15.98 | 38.01 | 58.72 | 271.32 | 1295.40 | 305.74 |
| Unused land to unused land | 181,728.90 | 181,538.49 | 181,592.80 | 169,179.04 | 173,228.86 | 171,350.03 |